12-2019

Electropermeabilization Does Not Correlate with Plasma Membrane Lipid Oxidation

Olga Michel

Andrei G. Pakhomov

Maura Casciola

Jolanta Saczko

Julita Kulbacka

See next page for additional authors

Authors

Olga Michel, Andrei G. Pakhomov, Maura Casciola, Jolanta Saczko, Julita Kulbacka, and Olga N. Pakhomova

Bioelectrochemistry 132 (2020) 107433

Contents lists available at ScienceDirect

Bioelectrochemistry

journal homepage: www.elsevier.com/locate/bioelechem

Electropermeabilization does not correlate with plasma membrane lipid oxidation

Olga Michel [a,b,*], Andrei G. Pakhomov [a], Maura Casciola [a], Jolanta Saczko [b], Julita Kulbacka [b], Olga N. Pakhomova [a]

[a] Frank Reidy Research Center for Bioelectrics, Old Dominion University, 4211 Monarch Way, Norfolk, VA 23508, USA
[b] Department of Molecular and Cellular Biology, Wroclaw Medical University, Borowska 211A, 50-556 Wroclaw, Poland

ARTICLE INFO

Article history:
Received 7 August 2019
Received in revised form 20 November 2019
Accepted 22 November 2019
Available online 15 December 2019

Keywords:
Electropermeabilization
C11-BODIPY
Oxidation
TIRF microscopy

ABSTRACT

The permeabilized condition of the cell membrane after electroporation can last minutes but the underlying mechanisms remain elusive. Previous studies suggest that lipid peroxidation could be responsible for the lasting leaky state of the membrane. The present study aims to link oxidation within the plasma membrane of live cells to permeabilization by electric pulses. We have introduced a method for the detection of oxidation by ratiometric fluorescence measurements of BODIPY-C11 dye using total internal reflection fluorescence (TIRF) microscopy, limiting the signal to the cell membrane. CHO-K1 cells were cultured on glass coverslips coated with an electroconductive indium tin oxide (ITO) layer, which enabled electroporation with micro- and submicrosecond pulses. No oxidation was observed with the electric field directed towards the ITO (cathode), even at field strengths much higher than that needed for permeabilization. Oxidation was readily detectable with the opposite polarity of pulses, but with the threshold higher than the permeabilization threshold. Moreover, a decrease in the medium conductance had opposite effects on permeabilization and lipid oxidation (it enhanced the former and suppressed the latter). We conclude that lipid oxidation can indeed occur at the plasma membrane after electric pulses, but it is not the cause of lasting membrane permeabilization.

1. Introduction

The application of pulsed electric fields (PEFs) can lead to the formation of transient pores in lipid bilayers and, consequently, to increased permeability to certain compounds. This phenomenon, known as electropermeabilization, has many applications in biotechnology and medicine as it allows for the intracellular transfer of macromolecules such as cytostatic drugs [1–5] and DNA [3,6–8]. However, mechanisms underlying this process are not fully understood. One of the unresolved puzzles is the long-lasting membrane permeability observed in cells following PEFs exposure. In experimental measurements, the membrane remains permeabilized for minutes [9–11], whereas the lifetime of electropores in molecular dynamics (MD) simulations is nanoseconds [12–14]. Lipid peroxidation has been hypothesized as a mechanism responsible for the prolonged permeability supported by experimental observations of changes in phospholipid conformation after PEFs treatment [14–17]. Theoretical models indicate that the oxidation of membrane components lowers the energy barrier required for electropermeabilization [18,19]. Experimental studies have shown that the application of PEFs is associated with the extracellular [20] and intracellular production of reactive oxygen species (ROS) [20–22]. Furthermore, the generation of ROS is not homogeneous over the cell surface but specific to the electropermeabilized, peripheral part of the cell [23]. The increased susceptibility to electropermeabilization of oxidized model membranes together with PEFs-evoked oxidation measured experimentally led to a hypothesis that oxidation can be a critical mechanism of PEFs action [16]. Maccarrone et al. [17] proposed that lipid peroxidation induced by electric pulses is associated with greater membrane fluidity, hence the oxidation parallels the enhanced membrane permeability. Here, we test the hypothesis that oxidation is the cause of sustained membrane permeabilization after the exposure to pulsed electric fields. Contradictory to this hypothesis, we demonstrate no causal relationship between lipid oxidation and electropermeabilization.

Lipid peroxidation is a consequence of oxidative stress and can have a significant impact on cell physiology. Oxidation of polyun-

* Corresponding author at: Department of Molecular and Cellular Biology, Wroclaw Medical University, Borowska 211A, 50-556 Wroclaw, Poland.
E-mail address: olga.michel@umed.wroc.pl (O. Michel).

https://doi.org/10.1016/j.bioelechem.2019.107433
1567-5394/

saturated fatty acids (PUFA) can lead to the decreased membrane fluidity, increased membrane permeability and inactivation of receptors and proteins, including transporters [24]. Three different approaches are used to detect oxidative stress in cells: (1) measurement of ROS (2) detection of oxidatively damaged molecules, and (3) analysis of cellular antioxidant defense systems. Methods to directly measure ROS include the detection of superoxide anion (O_2^-) (such as nitroblue tetrazolium reduction assay or cytochrome *C* reduction assay), detection of hydroxyl radical (e.g. deoxyribose degradation assay and aromatic hydroxylation assay), detection of singlet oxygen (via chemiluminescence, para-nitrosodimethylaniline bleaching method, iodide method), or the electron paramagnetic resonance (EPR) spin trapping, which is considered the most accurate method for free radicals' tracking [25–27]. Disadvantages of direct ROS measurements are low specificity and short half-life of radicals as well as the action of antioxidant systems. Therefore, it is preferred to detect oxidation via measurement of its secondary products such as malondialdehyde, 4-hydroxynonenal, isoprostanes, lipid-protein adducts or DNA damage [26,28–30]. Although detected products are more stable than free radicals, these methods are also limited by low specificity and often require cell fixation or extraction of their components for the more accurate measurement via chromatography or mass spectrometry [31]. However, the recent development of microscope-based methods has enabled observation of oxidation in live cells and organisms [32]. These include ratiometric measurements with fluorescent probes such as C11-BODIPY(581/591) which is described in detail below. Another approach is to assess activation of the antioxidant defense mechanisms protecting biological systems from oxidative damage. This applies mainly to direct-acting enzymes such as glutathione peroxidase, superoxide dismutase, or catalase [33–35] but may also include low-molecular-weight antioxidants like glutathione or vitamins [34,36,37]. The aforementioned techniques provide information on general oxidative stress in living cells, but rarely allow for the precise tracking of oxidation process at subcellular levels.

C11-BODIPY(581/591) is a fluorescent fatty acid analog in which phenyl moiety is connected to a 4,4-difluoro-4-bora-3a,4a-diaza-s-indacene (difluoroboron dipyrromethene, BODIPY, BP) core through a conjugated diene [38]. BODIPY probes have characteristics useful for live cell imaging including low sensitivity to environmental changes, excitation and emission in the visible spectral range, high fluorescence quantum yield, narrow emission bandwidth, and lipophilic character enabling the penetration of biological membranes [38,39]. BODIPY probes can be modified for specific tasks by the addition of residues in appropriate positions of the BODIPY core – as it is in the case of C11-BODIPY(581/591) where the attachment of the phenyl moiety shifts the fluorescence emission peak from green to red and makes it sensitive to oxidation [38,40]. Unfortunately, the mechanism by which oxidation acts on BP dye remains unclear. There is abundant evidence that BP oxidation is not caused by the initiators of the lipid peroxidation but rather by a variety of oxy-radicals and peroxynitrate [38,41], and that different products may be formed depending on the oxidant used [42]. Another controversy relates to C11-BODIPY (581/591) sensitivity to oxidation. Several studies concluded that C11-BODIPY(581/591) is a valuable tool to quantify lipid oxidation in biomembranes [38,42–44]. However, mass spectrometry analysis has suggested that C11-BODIPY(581/591) has higher susceptibility to oxidative damage than 1-stearoyl-2-arachidonyl-*sn*-glycero-3-phosphocholine (SAPC) and therefore underreports the antioxidant effect of α-tocopherol [45]. Moreover, the probe exhibits an antioxidant effect by itself [45]. Pap et al. [46] identified several pitfalls of applying BODIPY for quantification of oxidant activities and effectiveness of antioxidants, namely probe leakage after long incubation, quenching and excimer formation at high mole fractions, photooxidation by high intensity excitation light, and heterogeneous distribution within the sample.

Up to now, heterogeneous distribution of the dye within cells precluded the use of C11-BODIPY(581/591) for tracking the plasma membrane lipid oxidation, as the collected signal came from both external and internal membranes. In order to overcome this limitation, we decided to employ a technique which restricts the excitation to cell plasma membrane and thereby increases the signal-to-noise ratio. Total internal reflection fluorescence (TIRF) microscopy restricts detection of fluorescence to a thin 90–150 nm region at the interface between a glass coverslip and medium. For a comprehensive review of theoretical principles and rational for its application in biological studies, readers are referred to Mattheyses [47] and Axelrod [48,49]. In brief, this technique is based on the adjusting the excitation light to the "critical angle", totally reflecting all of the excitation light away from the sample, but creating an evanescent wave at the interface, capable of exciting fluorophores within 100 nm above the glass surface. By creating an evanescent wave with a very short propogation distance TIRF imaging enables thinner optical slicing and better separation of the signal from the cell membrane than confocal microscopy [47]. TIRF microscopy has been successfully employed in studies on focal adhesions [50], cytoskeleton [51–53], calcium channels [54], granulation and exocytosis [55–57]. Furthermore, rapid acquisition achievable with TIRF enabled tracking of dynamic morphological changes in protein-coated emulsion particles [58] and nanoscale imaging of domains in supported lipid membranes [59]. Overall, TIRF microscopy has become a powerful tool for studying dynamic processes at the cell surface. In the present study, we combined TIRF technology with C11-BODIPY(581/591) fluorescent staining in order to observe plasma membrane lipid oxidation following the delivery of electric pulses.

2. Material and methods

2.1. Cell culture

Experiments were performed in a CHO-K1 cell line from a Chinese hamster ovary (ATCC, Manassas, VA). Cell culture was maintained in a CO_2 incubator at 37 °C in Ham's F-12 K medium supplemented with L-glutamine (Corning, Christiansburg, VA) with the addition of 10% fetal bovine serum (Atlanta Biologicals, Norcross, GA) and antibiotics: 100 IU/ml penicillin, and 0.1 mg/ml streptomycin (Gibco, Gaithersburgh, MD). For experiments, cells were detached with 0.25% trypsin-EDTA (Gibco), resuspended in the growth medium, and seeded at ~0.5×10^4 cells in glass-bottomed 35 mm Petri dishes (MatTek, City, State). We utilized both standard dishes with Poly-D-Lysine-coated glass (cat. # P35GC-1.0–14-C) and dishes with a transparent electroconductive indium-tin oxide (ITO) layer on the top of the glass. Custom dishes were fabricated by MatTek using 15 mm diameter glass coverslips covered with ITO to the sheet resistance of 8–12 Ohm/sq by Diamond Coatings Ltd. (Halesowen, UK). The ITO surface was coated with poly-L-lysine (Sigma-Aldrich, St. Louis, MO) to improve cell adherence. Biocompatibility of the ITO-coated glass coverslips has been demonstrated in our previous studies on nsPEFs [60,61].

2.2. Reagents and staining protocols

BODIPY™ 581/591 C11 (BP) was purchased from ThermoFisher Scientific (Middletown, VA) as part of the Image-iT® Lipid Peroxidation Kit. The optimal staining time was chosen based on experiments comparing signal measured from the membrane (in the TIRF mode) to signal measured from whole cell illumination (in the widefield mode). The concentration of BP used for staining was 5 μM in all protocols.

Cumene hydroperoxide (CH-OOH) at concentrations of 25–100 μM was used to examine the dye's oxidation in TIRF mode compared to widefield epifluorescence. Staining and incubation with the oxidizer were performed at 37 °C. For optimization of a method we tested various oxidation protocols: (A) Cells were incubated with BP and complete culture medium (CCM) with CH-OOH for 5 min; (B) Cells were incubated for 1 h with CH-OOH in CCM, then washed 3 times with PBS buffer and incubated for 5 min with BP in CCM; (C) Cells were incubated with CH-OOH for 1 h, then BP was added to the solution to a final concentration of 5 μM; and (D) 5 mM BP were incubated in a cell-free CCM with 100 μM CH-OOH for 1.5 h, then diluted with CCM to a final concentration of 5 μM BP and 0.1 μM CH-OOH. Cells were stained with the diluted solution for 5 min. Each protocol ended with 3 PBS washes and addition of the appropriate solution (Tyrode solution or for some experiments a low conductivity solution) for measurements.

All dye uptake and oxidation measurements were performed in a standard Tyrode's solution composed of (in mM): 140 NaCl, 5.4 KCl, 2 $CaCl_2$, 1.5 $MgCl_2$, 10 dextrose, and 10 HEPES; pH 7.3, ~300 mOsm/kg, conductivity 15 mS/cm. All chemicals were purchased from Sigma–Aldrich (St. Louis, MO) unless noted otherwise. In some experiments, we used a low-conductance solution (conductivity 1.3 mS/cm) prepared by mixing 1 part of Tyrode's solution with 9 parts of isosmotic sucrose solution in water.

1 μM YO-PRO-1 (Life Technologies, Grand Island, NY) and 5 μM Calbryte™ 520 AM (AAT Bioquest, Inc., Sunnyvale, CA) were used to determine cell permeability. Poorly permeant YO-PRO-1 was present in the solution surrounding adherent cells at the time of pulse application. As dye fluorescence increases after binding to DNA [62], the fluorescence signal was detected only from electropermeabilized cells. Calbryte™ 520 AM is a cell-permeable calcium indicator. Cells were loaded with the dye for 25 min at room temperature in the dark and washed 3 times with PBS. Next, cells were treated with PEFs in Tyrode's solution containing 2 mM Ca^{2+} ions. Calbryte™ 520 emitted bright fluorescence when cytosolic levels of free Ca^{2+} increased. CHO-K1 cells do not express any voltage-gated Ca^{2+} channels, and therefore cytosolic Ca^{2+} increase serves as a sensitive marker of cell membrane electropermeabilization [63–65].

2.3. PEFs exposure methods and protocols

A Petri dish with cells on the ITO coverslip was filled with either Tyrode's solution or low conductivity medium and placed in a holder on a motorized stage of an Olympus IX83 inverted microscope (Olympus America, Center Valley, PA). A selected target cell or a compact group of cells was brought to the center of the field of view. A tungsten rod electrode (100 μm diameter) was positioned above the target cells, precisely 100 μm above the coverslip and at 35° to the horizontal plane, by means of a robotic micromanipulator (model MPC-200, Sutter Instrument, Novato, CA). The bare tip of an otherwise insulated flexible silver wire was brought in contact with the ITO layer at a random spot remote from target cells. The wire and the rod were connected to a chosen PEFs source to deliver a vertical electric fields to target cells (Fig. 1A).

The electric field (E) distribution was calculated with COMSOL Multyphysics, Release 5.0 (COMSOL Inc., Stockholm, Sweden) in quasi-static conditions with the Electric Currents interface, similarly to what was previously described [66,67]. A tungsten rod electrode (100 μm diameter, 1 mm height with conductivity 18.94×10^6 S/m) was placed at an angle of 35° at 100 μm above glass coverslip. The coverslip was modeled as a dielectric cylinder of 4 mm diameter, 100 μm thickness with conductivity 0 S/m and relative permittivity of 3.78. The top side of the glass coverslip was simulated with conductivity of 1.3 MS/m to mimic the electric characteristics of ITO [68]. The electrodes were immersed in a solution with the conductivity of 1.4 S/m and relative permittivity of 76 to model the medium used in experiments. The set-up described (Fig. 1A) was surrounded by a 6 mm diameter sphere of air.

A tetrahedral mesh chosen to discretize the domain of simulation resulted in a mesh element minimum size of 9 μm, a maximum size of 210 μm, and a total of 364,408 elements. Quadratic elements were used throughout the solution domain, giving 493,259 degrees of freedom. The electric field was calculated applying 1 V to the rod electrode, while the ITO surface was grounded. Fig. 1B. shows the electric field distribution calculated in the xy plane above the ITO surface as well as the region of interest (ROI). The mean intensity of the electric field in the ROI was 0.048 kV/cm and its coefficient of variation was 9%, showing a high homogeneity of the electric field distribution. The application of 1 V to the ITO surface while the rod electrode was grounded did not change the results in terms of electric field distribution. However, the electric field lines had, as expected, the opposite direction (data not shown).

Single, trapezoidal 300 ns pulses of 2.4–24 kV/cm were delivered to cells with a custom made generator [69] driven by a BNC Model 577 digital delay generator and charged from a high voltage power supply (Bertan Associates, Model 215). The delay generator was used either for the delay generation when nsPEFs were applied or as a pulse generator for μsPEFs application. 100 μs pulses of electric field strength ranging from 0.24 to 0.72 kV/cm were delivered as a single pulse or train of 8 pulses with 5 kHz frequency. In the last case, the maximum adiabatic heating for the highest amplitude did not exceed 1.5 °C.

Pulse shape and amplitude were monitored using a 100 MHz oscilloscope (DSO-5102P, Hantek, Qingdao, China) and a voltage probe (PP-80, Hantek). Axon Digidata 1550B board and pClamp 10 software (Molecular Devices, San Jose, CA) were used to control and synchronize image acquisition and pulse delivery. Start of the image acquisition, pulse repetition rate, and time of pulse delivery were all programmed in pClamp. Metamorph software v. 7.10.2.240 (Molecular Devices) was used to set the sequence of acquisition.

2.4. Widefield and TIRF fluorescence imaging

Our IX83 microscope was equipped with a cell TIRF MITICO unit (Olympus), PlanApo N 60x/1.45 oil TIRF objective (Olympus), Orca Flash 4.0 V.3 sCMOS camera (Hamamatsu, Bridgewater, NJ), and 488 nm and 561 nm excitation lasers (both 100 mW; Coherent, Santa Clara, CA).

Calbryte (a cytosolic Ca^{2+} indicator) and YO-PRO-1 (cell-impermeable nucleic acid stain) fluorescence was measured in widefield mode, excitation with a 488 nm laser, using a FITC cube and EGFP clean-up filter with center wavelength at 470/40 nm (model 49002, Chroma Technology, Bellows Falls, VT). Time lapse imaging was triggered 4–20 s before the exposure and continued for 100–300 s. Calbryte data were normalized to frames obtained prior to exposure and YO-PRO-1 data were corrected by background subtraction.

Fluorescence of C11-BODIPY was measured in both widefield and TIRF modes. All electropermeabilization experiments were imaged using the TIRF mode, which was controlled by the Olympus CellTIRF 1.4 software. Oxidized dye was excited with the 488 nm laser and fluorescence was detected using the FITC cube and 470/40 clean-up filter, similarly to YO-PRO-1 and Calbryte. Non-oxidized dye was excited with the 561 nm laser using a TX Red cube and a 560/40 nm clean-up filter (model 49008, Chroma). The degree of oxidation (DO) of BODIPY dye was determined as a percent difference of the oxidized dye fluorescence intensity ($F_{488/525}$) to the total fluorescence defined as the sum of the oxidized and reduced dye fluorescence ($F_{561/605}$)::

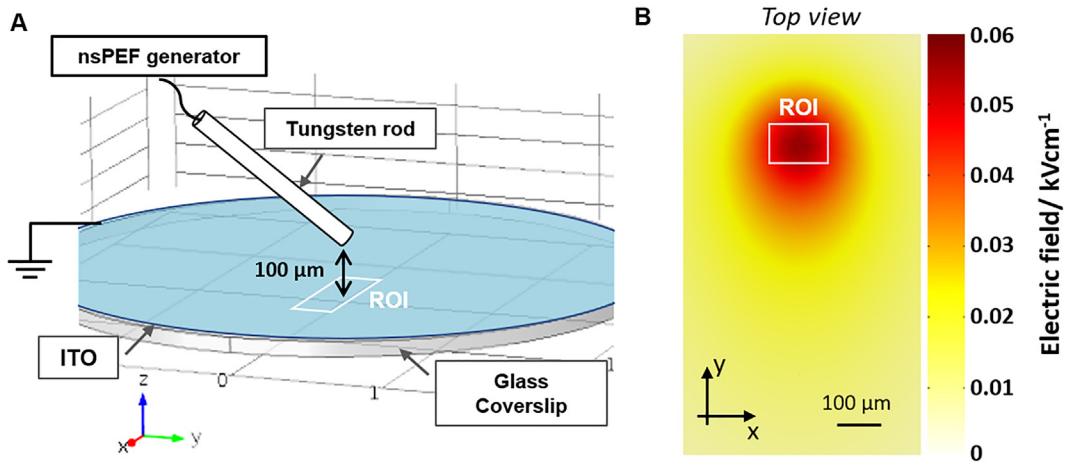

Fig. 1. Electrode arrangement to expose the cell membrane adherent to the coverslip. (A) A schematic of the experimental set-up. (B) Electric field distribution in the xy plane (z = 0 µm) parallel to the ITO surface. A region of interest (ROI) (140 × 90 µm) shows a high electric field intensity (0.048 $kVcm^{-1}$ for 1 V applied), as well as good homogeneity (see text).

$$DO = \frac{F_{488/525}}{F_{561/605} + F_{488/525}} \quad (1)$$

Emission signals were separated by Lambda 10–2 filter wheel (Sutter Instrument) switching between 605/52 nm and 525/36 nm emission filters synchronously with alternating activation of 561 and 488 nm lasers, respectively. The lasers were operated at 1% (561 nm) and 10% (488 nm) of full power; the exposure time at each wavelength was 23 ms. The multiwave acquisition cycle was controlled by Metamorph software triggered by a pClamp protocol. Two images were collected per time-point – one from the 561 nm channel and one from the 488 nm channel (with the exact order of acquisition). In each experiment data were collected at three time-points: 4 s before, 1 s after, and 6 s after pulse delivery resulting in 6 total images from each experiment. Data were analyzed after background subtraction for each channel (488 and 561 nm) separately.

Fluorescence intensity was quantified with the Fiji package of ImageJ software [70]. Images acquired with a DIC prism were used to mark regions of interest and transposed to fluorescence images.

Numerical data were analyzed and presented with Microsoft Excel and GraphPad Prism 7 (La Jolla, CA). All experiments were replicated 3–5 times in a minimum of three separate sets of experiments. The results are presented as a mean +/- standard error (s.e.). Statistical analyses were performed using a two-tailed *t*-test or one-way ANOVA followed by Dunnett's multiple comparisons test, with $p < 0.05$ considered statistically significant.

3. Results

3.1. C11-BODIPY$^{581/591}$ staining

In classic epifluorescence (referred to as "widefield") the laser beam penetrates the sample exciting all fluorochromes within the focal volume. It has been demonstrated that C11-BODIPY (581/591) is distributed heterogeneously throughout the cell membranes, with predominant staining in the perinuclear region and mitochondria [38]. Consequently, the fluorescence changes measured in widefield mode cannot be attributed to plasma membrane alone. TIRF microscopy overcomes this by restricting the excitation region to thin (tens of nanometers) layer enabling observation of processes at the plasma membrane. In the present study, we tested different staining times – we incubated cells with C11-BODIPY for 5, 15 or 30 min at 37 °C and compared the fluorescent signal obtained in widefield mode to TIRF mode. Five minute incubation appeared to be suitable labeling time, allowing for the visualization of membranes in both widefield and in TIRF mode (Fig. 2).

We evaluated the influence of labeling time on the emission from the membrane (F_{TIRF}) and the emission from the whole cell (F_{WF}). We observed that a shorter incubation time yielded more dye in the plasma membrane as compared to the whole cell (Table 1).

3.2. C11-BODIPY$^{581/591}$ oxidation

It has been demonstrated that conjugated diene connecting the phenyl moiety with the BODIPY core is a target for free radical-mediated oxidation [42]. However, data on the response of BODIPY to different oxidative systems within living cells are contradictory [38,40–42,71]. Here, we tested various protocols to establish a positive control for BODIPY-C11 oxidation. For initiation of oxidation process in cells we used 50 µM cumene hydroperoxide (CH-OOH) – compound known to induce a lipid peroxidation [72,73]. We examined if the time of incubation with CH-OOH influence the oxidation of the BODIPY and if the oxidizer needs to be present in the cell solution during staining.

Compared to cells incubated for 1 h with a complete culture medium (Fig. 3A), a short 5-minute incubation with 50 µM CH-OOH did not increase BODIPY oxidation (Fig. 3B). We concluded that for such a short time and sublethal CH-OOH dosage, lipid peroxidation is either countered by cell antioxidant systems or C11-BODIPY is not sensitive enough to detect such a minor oxidation.

Furthermore, we examined if endogenous ROS production affects the degree of BP oxidation. For that purpose, we extended time of incubation with the oxidizer, but removed the oxidizer prior to BODIPY staining. Another approach for endogenous ROS generation was depriving cells of fetal bovine serum, which is known to mitigate induced oxidative stress [51,52]. Incubation for 1 h followed by cell wash and staining did not increase the degree of BP oxidation (Fig. 3C). On the other hand, we detected slightly higher oxidation in cells treated with FBS-free solution but only in the TIRF mode (Fig. S1).

Finally, when cells were incubated for 1 h with 50 µM CH-OOH and BP was added to this solution without a wash increased degree of BP oxidation was observed in both widefield and TIRF mode (Fig. 3D).

Once we determined conditions that caused C11-BODIPY oxidation we tested its sensitivity to various concentrations of cumene

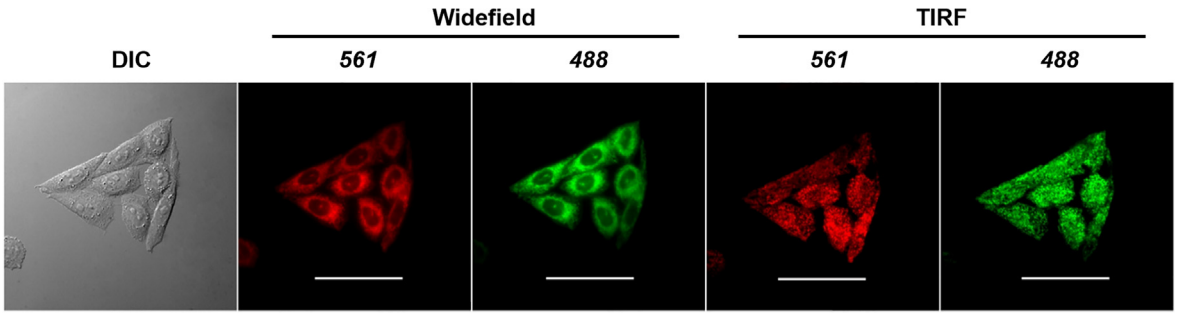

Fig. 2. Representative images of CHO-K1 cells stained for 5 min with C11-BODIPY, as recorded with differential interference contrast (DIC), classic epifluorescence (widefield) and total internal reflection fluorescence (TIRF) miscroscopy at the penetration depth of 100 nm. The scale bar is 50 μm.

Table 1
The influence of the staining time on the relative fluorescence of C11-BODIPY, as measured in widefield (WF) and in TIRF mode. F_{TIRF}/ F_{WF} is the ratio between fluorescence emission in TIRF and WF mode for each excitation wavelength. Shorter incubation results in a better accumulation of BODIPY in the plasma membrane (reflected by a higher F_{TIRF}/F_{WF} ratio).

	561 nm			*488 nm*		
	F_{TIRF}	F_{WF}	F_{TIRF}/F_{WF}	F_{TIRF}	F_{WF}	F_{TIRF}/F_{WF}
5 min	3323	10,989	0.30	2447	4371	0.56
15 min	3209	10,572	0.30	2115	4737	0.45
30 min	3731	23,464	0.16	2869	9254	0.31

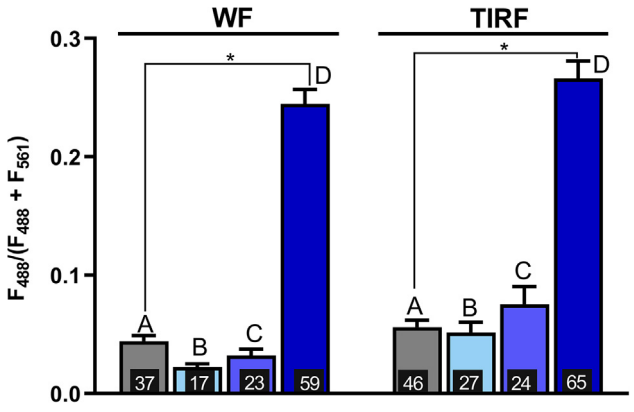

Fig. 3. The degree of oxidation of BODIPY-C11 probe (BP) following different oxidation protocols as measured with widefield (WF) and TIRF microscopy. (A) Control cells incubated with a complete medium, then BP was added to the solution for 5 min; (B) Cells incubated simultaneously with cumene hydroperoxide (CH-OOH) and BP for 5 min; (C) Cells incubated for 1 h with CH-OOH, then washed and stained with BP solution for 5 min; (D) Cells incubated for 1 h with CH-OOH then BP was added to solution for 5 min. The number of examined cells is provided at the bottom of each bar. One-way ANOVA with Dunnet's corrections was used for comparison between Control and CH-OOH-treated groups (*$p \leq 0.05$).

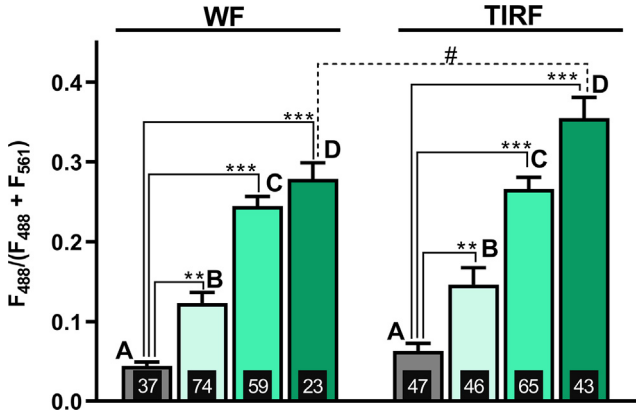

Fig 4. The degree of oxidation of C11-BODIPY in cells incubated with cumene hydroperoxide (CH-OOH) at concentrations of (in μM): 0 (A), 25 (B), 50 (C) and 100 (D). Emission was measured in widefield mode (WF) or in TIRF mode. The number of examined cells is provided at the bottom of each bar. One-way ANOVA with Dunnet's corrections was used for comparison between Control and CH-OOH-treated groups (**$p \leq 0.01$; ***$p \leq 0.001$) and between WF and TIRF modes (# $p \leq 0.01$).

hydroperoxide. The degree of BP oxidation was positively correlated with CH-OOH concentration as observed both in widefield and in TIRF modes (Fig. 4). Regardless of the applied CH-OOH concentration, the degree of BP oxidation measured in TIRF mode was higher than in widefield mode, however the difference was statistically significant only for 100 μM CH-OOH (*t*-test, # $p \leq 0.01$). Increase in BP fluorescence in TIRF mode can be explained by a higher level of oxidation at the plasma membrane compared to internal membranes.

To accurately determine oxidant activity in living cells, molecules reporting lipid peroxidation should respond to a variety of reactive oxygen species, but remain insensitive to hydroperoxides [38]. We examined if BODIPY oxidation can result from a direct interaction between the dye and CH-OOH molecule. We incubated BODIPY at 5 mM in cell-free solution with 100 μM CH-OOH for 90 min and then used for cell staining. Cells incubated with 50 μM CH-OOH treatment were used for positive control, as described in the previous section.

As measured in TIRF mode, degree of BP oxidation was almost identical for native (Fig. 5A) and CH-OOH pretreated dye (Fig. 5C). The lack of BODIPY oxidation directly by CH-OOH (in the absence of lipids) indicates that BODIPY probe truly reports the oxidation of lipids rather than a direct effect of the oxidizer on the dye.

3.3. Lack of oxidation at the cathode-facing portion of cell membrane

Having established the sensitivity of the dye to chemically induced oxidation and a positive control, we exposed cells to PEFs by placing them on an ITO coverslip under an electrode. In the first experiment, the electric field was directed from the return electrode towards the ITO layer beneath the cells. TIRF mode was used to image the cathode-facing portion of cell plasma membrane. We applied single 300 ns pulses at up to 25 kV/cm. Images were taken immediately before, at 1 s, 5 s and 10 s after pulse delivery. To evaluate longer durations, some recordings were made at 240 s after pulse delivery. For the sham-exposed control, all procedures remained the same, but pulse(s) were delivered at 0 kV/cm. The permeabilization thresholds for YO-PRO-1 (<7 kV/cm; Fig. 6A, n = 9–13 cells) and Ca^{2+} ions (<2.4 kV/cm; Fig. 6B, n = 9–17 cells)

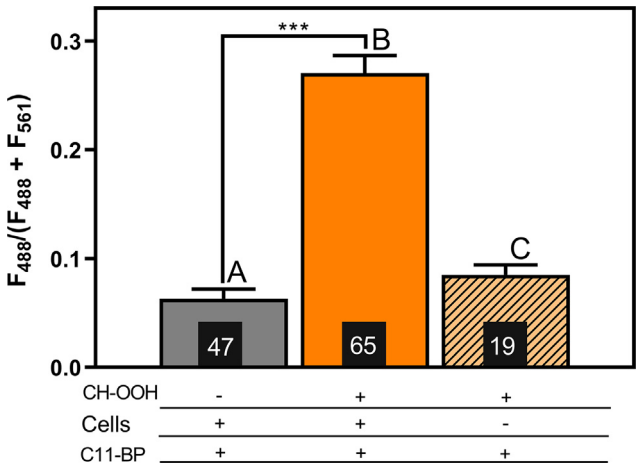

Fig. 5. C11-BODIPY detects membrane lipid oxidation but is insensitive to the direct action of CH-OOH. The TIRF mode was used to measure oxidation in cells incubated with a complete culture medium for 65 min (A), cells incubated for 60 min with 50 μM CH-OOH and further for 5 min with 5 μM BODIPY added to the solution (to final 5 μM) (B) or in cells stained with 5 μM BODIPY incubated for 90 min with 100 μM CH-OOH prior to staining (C). The number of examined cells is provided at the bottom of each bar. One-way ANOVA with Dunnet's corrections was used for comparison between Control and CH-OOH-treated groups (*** $p \leq 0.01$).

did not correlate with the lipid oxidation, which was detected at 10 s after pulse delivery (Fig. 6C, n = 11–19 cells) only at high electric fields. Such high intensities of electric field caused severe blebbing, pyknosis, and cell granulation (data not shown). Within the studied limits, we did not detect any oxidative response in the cathode-facing membrane immediately after pulse delivery (Fig. 6C) at any electric field intensity.

This result suggests that electropermeabilization was not caused by lipid oxidation. However, changing the electric field direction (making ITO anode) drastically changed the outcome of measurements and enabled consistent detection of lipid oxidation by pulses. Therefore, this configuration (imaging of anode-facing membrane portion) was employed for all experiments detailed below.

3.4. Lipid oxidation at anode-facing membrane side and YO-PRO-1 dye uptake in a standard Tyrode's solution.

When the electric field polarity was changed and ITO acted as the positive electrode during pulses, we observed a statistically significant ($p < 0.001$) lipid oxidation at 5 s of measurement (1 s after electric pulse delivery) and its enhancement after next 5 s (Fig. 7). Oxidation was caused by all three tested pulse modalities but at different electric field strengths.

The threshold for oxidation was between 12 and 14.4 kV/cm (one 300 ns pulse), between 0.48 and 0.6 kV/cm (one 200 μs pulse), and between 0.24 and 0.36 kV/cm (eight 100 μs pulses at 5 kHz). These electric fields treatments caused severe (300 ns) or moderate (100 μs) morphological changes that developed within seconds after the treatment (Fig. 7, insets) matching previously described cytophysiological effects of membrane permeabilization and cell damage by ultrashort electric pulses [60,74].

For a single 300 ns pulse, cell membrane permeabilization threshold (measured by YO-PRO-1 uptake) was below 4.8 kV/cm (Fig. 8A), which is much lower than required for lipid oxidation. This result may indicate that permeabilization occurred without oxidation, or that oxidation was just too weak to be detected. In contrast, for pulses of 100 μs duration YO-PRO uptake thresholds were close to those required for membrane oxidation, specifically

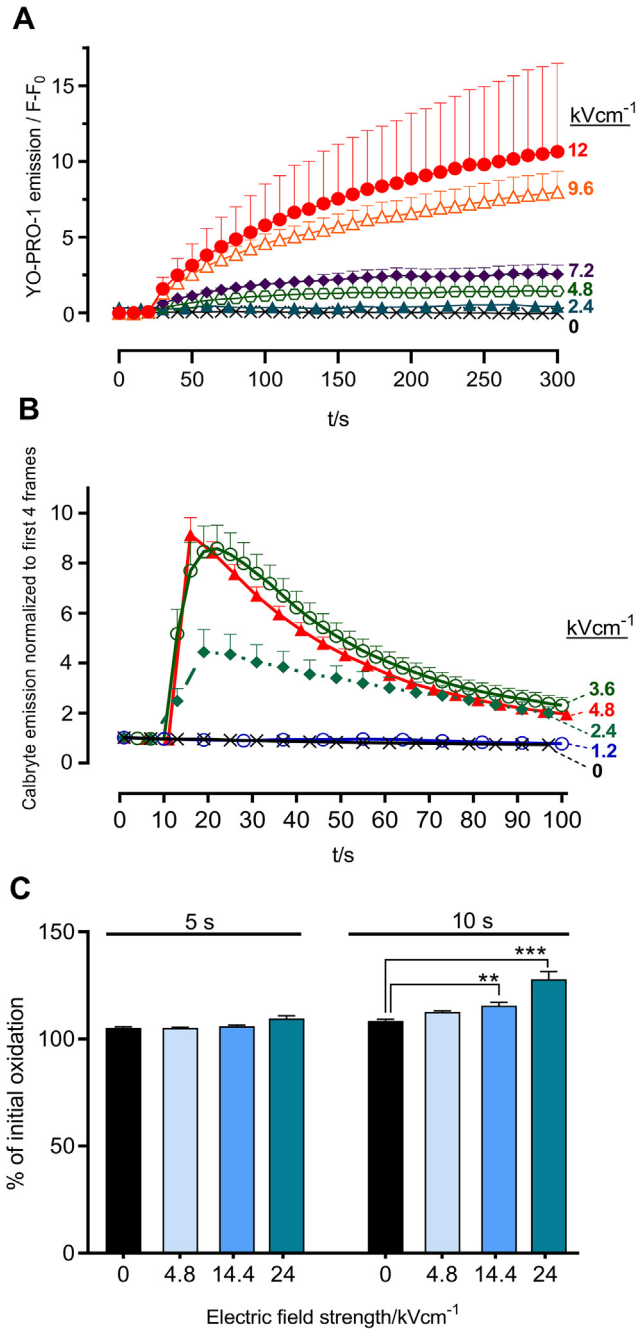

Fig. 6. Permeabilization of the cell membrane to YO-PRO-1 (A) and Ca^{2+} (B) is not accompanied by the oxidation at the cathode-facing portion of the cell membrane (C). Cells bathed in Tyrode's solution were exposed to a single 300-ns pulse at the indicated electric field strength at 20 s (A) or 10 s (B) into the experiment. Permeabilization was detectable already in 10 s after a 4.8–12 kV/cm pulse (A) and in 2 s after a 2.4–4.8 kV/cm pulse (B). However, no oxidation was detectable in 5 s even at much higher electric field strengths, up to 24 kV/cm (C). A statistically significant increase in the membrane oxidation (** $p \leq 0.01$; *** $p \leq 0.001$) occurred only in 10 s after the pulse and at the highest electric field strengths of 14.4 and 24 kV/cm.

0.48 kV/cm for a single pulse (Fig. 8B) and between 0.27 and 0.36 kV/cm for eight 100 μs pulses (Fig. 8C).

These experiments showed that lipid oxidation may indeed take place shortly after PEFs application but did not test if it was the cause of permeabilization. At first examination, the lack of oxidation at the cathode-facing side of the cell and PEFs-related dye uptake at electric field levels below an observable oxidation threshold point to the lack of causal relation. Lipid oxidation could

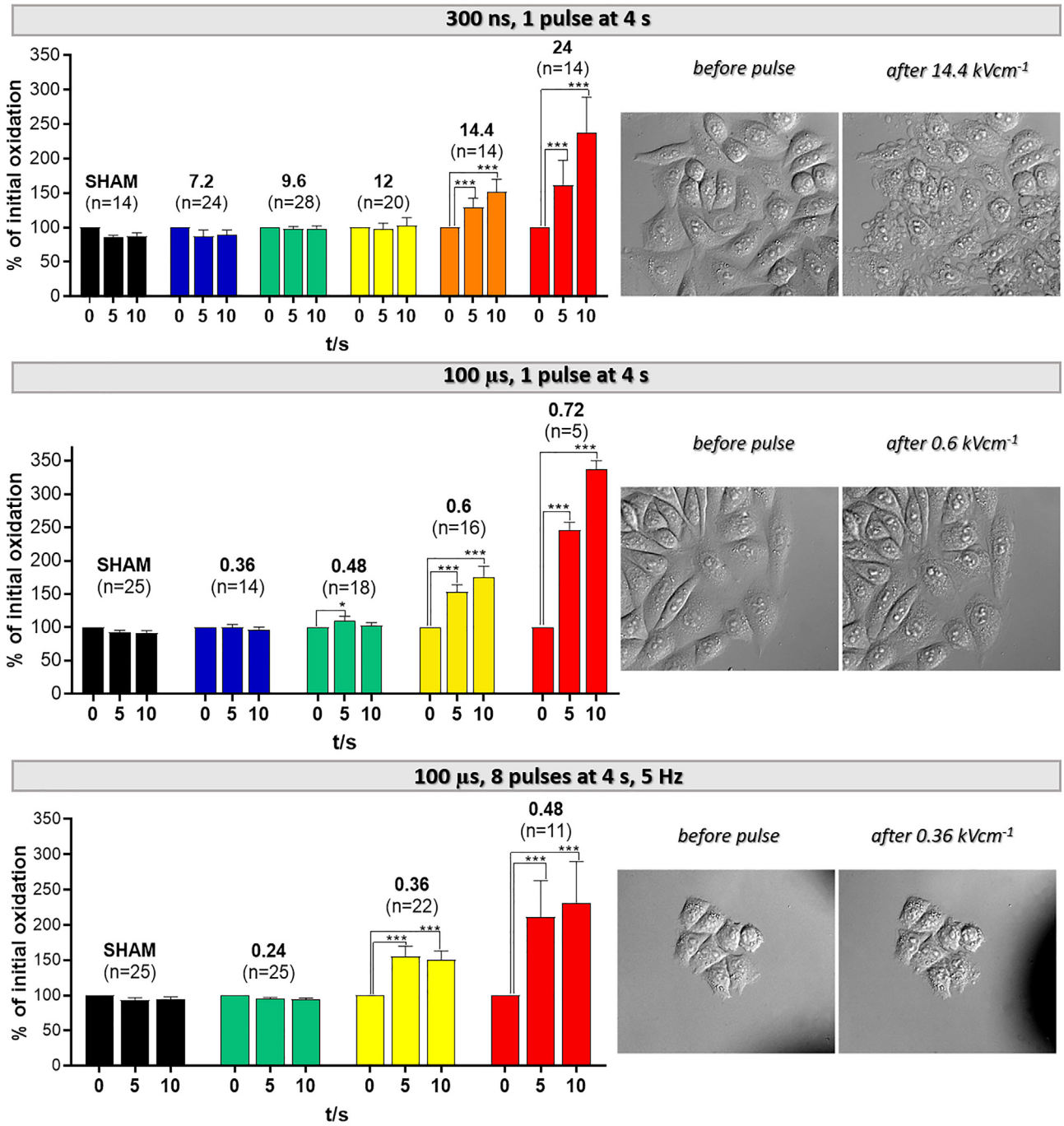

Fig. 7. Oxidation of the plasma membrane by anodic electric pulses of different duration and intensity. The dye's $F_{488}/(F_{561} + F_{488})$ emission ratio in each individual cell prior to pulse delivery was taken as 100% and plotted as mean +/− s.e. Two-tailed student *t*-test was employed to identify statistically significant differences in oxidation (*$p \leq 0.05$; ***$p \leq 0.001$ compared to 100%). Insets show representative DIC images of cells before and 10 s after the exposure at indicated field strength. Scale bars are 20 µm.

be a "byproduct" of electroporation, as a consequence of inevitable electrochemical reactions at the anode, which may or may not affect the degree of permeabilization but are not the cause of it. To examine this possibility a series of experiments were performed to compare YO-PRO-1 fluorescence to the degree of oxidation in a reduced conductivity medium.

3.5. Decreasing medium conductivity enhances permeabilization but inhibits lipid oxidation

It is well known that the yield of electrochemical reactions is directly proportional to the current flowing through the medium [75,76]. Hence, reduction of medium conductivity would reduce current and consequently, if it is indeed a product of electrochemical reactions, reduce lipid oxidation. By extension, if permeabilization is caused by oxidation, permeabilization should also be suppressed. Previous studies reported both stronger [77–79] and weaker permeabilization [80] in lower-conductance medium, hence we needed to test the effect of medium conductance on oxidation and permeabilization specifically for our exposure conditions.

Fig. 9 shows that delivering electric pulses in a low-conductance medium significantly enhanced YO-PRO-1 uptake for all tested pulse modalities (single 300 ns and 100 µs pulses

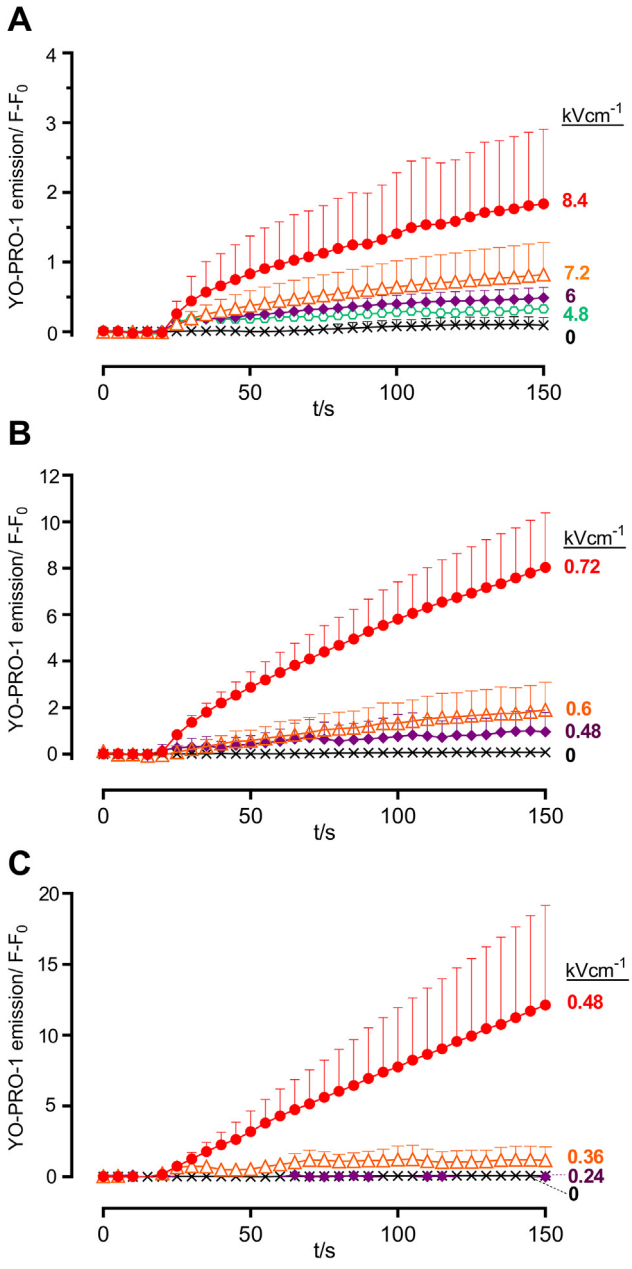

Fig. 8. YO-PRO-1 uptake in cells bathed in Tyrode's solution and exposed to a single 300 ns (A) or 100 μs pulse (B), or to eight 100 μs pulses at 5 kHz (C) at 20 s into the experiment. Pulse was delivered to the anode-facing portion of cell membrane. Images were acquired every 5 s in the widefield mode. Data were collected in 3–5 independent experiments (10–23 cells/group) and presented as mean ± s.e.; error bars are shown in one direction only for clarity.

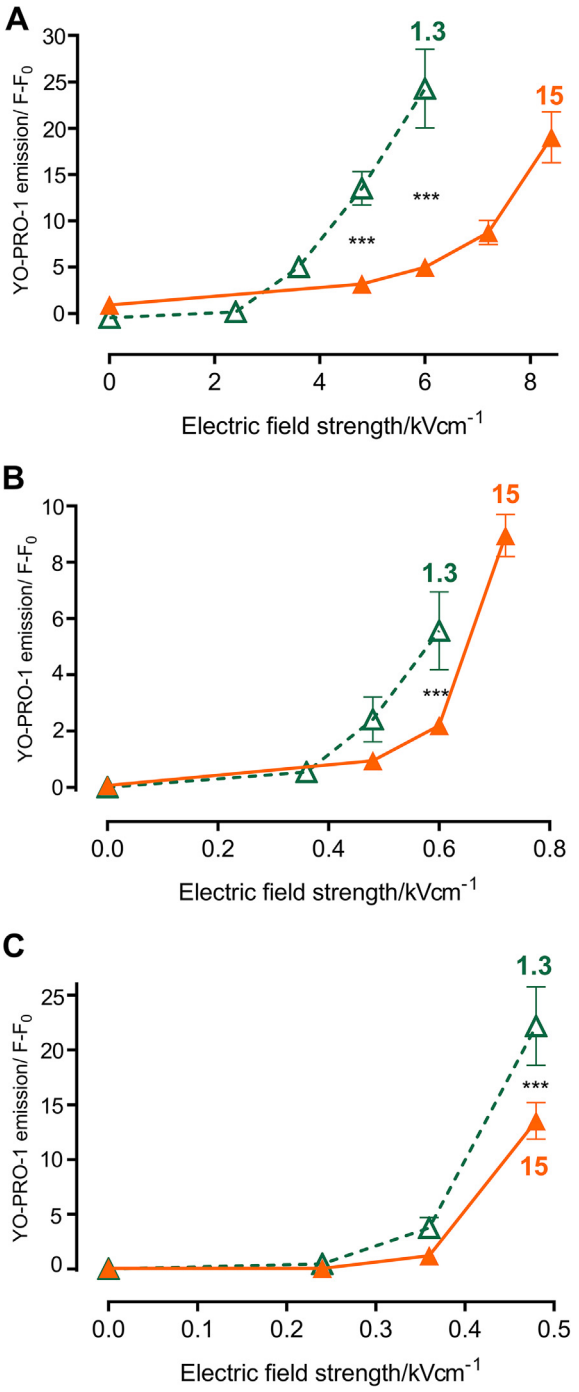

Fig. 9. Cell electropermeabilization to YO-PRO-1 is enhanced in a low-conductance solution. YO-PRO-1 emission was measured in cells bathed in either 15 (—) or 1.3 (– –) mScm^{-1} solution 130 s after the exposure to single 300 ns pulse (A), to one 100 μs pulse (B), or to a 5 kHz train of eight 100 μs pulses (C). One-way ANOVA with Dunnet's corrections was employed to examine differences between media of higher and lower conductance (*** $p \leq 0.001$).

and trains of eight 100 μs pulses), with or without lowering the electric field threshold. On the contrary, lipid oxidation was strongly inhibited (as was expected for an electrochemical reaction yield), and its threshold increased (Fig. 10). With 300 ns pulses, we could not detect oxidation in a low-conductance solution within the entire tested range of field strengths (Fig. 10A, B). Moreover, without having any effect on lipid oxidation, pulse amplitudes higher than required for increased permeabilization to YO-PRO affected cell morphology, which was manifested by granulation, pyknosis or even immediate destruction of the cell membrane (Fig. S3).

The opposite effect of the solution conductivity on lipid oxidation and membrane permeabilization unequivocally proves that there is no causal relation between these two processes, although some impact of oxidation on the degree of permeabilization, membrane repair, and various downstream biological consequences of permeabilization cannot be excluded.

3.6. The anode-facing membrane is indeed the site of permeabilization by electric pulses

The conclusion that permeabilization is not caused by lipid oxidation might be erroneous if we measure oxidation at the lower

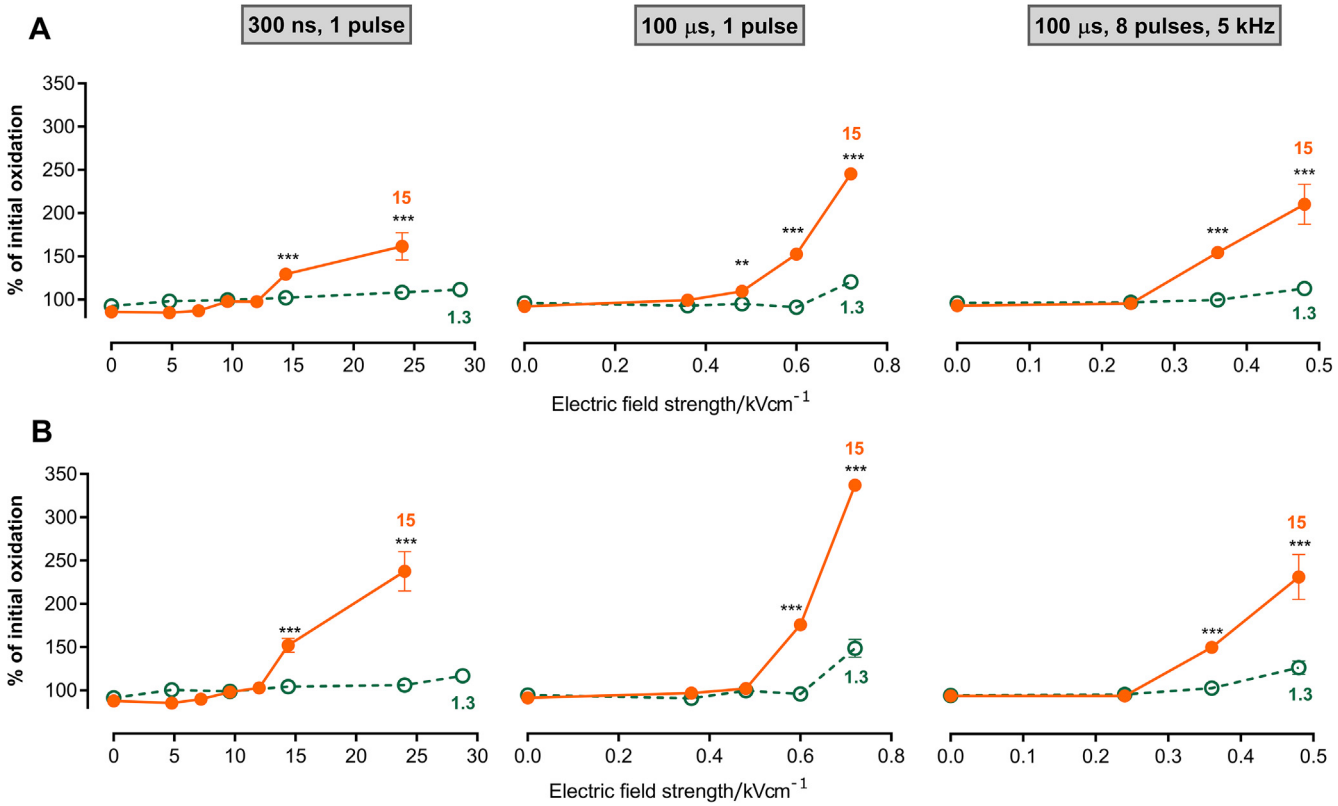

Fig. 10. Lipid oxidation is suppressed in a low-conductance solution. Degree of oxidation of C-11 BODIPY was measured in cells 1 s (A) or 6 s (B) after pulse delivery. Cells bathed in either 15 (—) or 1.3 (–) mScm^{-1} solution were exposed to one 300 ns pulse, to one 100 μs pulse or to a 5 kHz train of eight 100 μs pulses. One-way ANOVA with Dunnet's corrections was employed to examine differences between media of higher and lower conductance (**p ≤ 0.005; *** p ≤ 0.001).

(anode-facing) membrane while permeabilization somehow occurs exclusively at the top (cathode-facing) side of the membrane. While such selective permeabilization appears improbable, it cannot be immediately ruled out either. The experiments with YO-PRO-1 uptake (Figs. 8 and 9) provided no answer as to which exact side of the cell membrane was permeabilized, thereby requiring an additional experiment. We employed fast imaging of subplasmalemmal Ca^{2+} increase at the lower site of the cell to prove Ca^{2+} entry through the electropermeabilized lower membrane. Of note, CHO cells employed in this study express no endogenous voltage-gated channels [63], hence electroporation is only known pathway for fast Ca^{2+} entry after electric pulses [64,65].

Cells were loaded with Calbryte Ca^{2+} indicator and imaged in TIRF and widefield mode at 1 frame/s, starting 1 s before the pulse. The acquisition of the second frame started simultaneously with pulse delivery and continued for 23 ms. With 300 ns pulses, fast Ca^{2+} increase was already observed at field intensity as low as 2.4 kV/cm (Fig. 11). Most importantly, in TIRF mode Ca^{2+} increase was obvious already in the first frame after exposure, i.e., within less than 23 ms after the pulse (Fig. 11, top row); and considering the rolling shutter acquisition type of the employed sCMOS

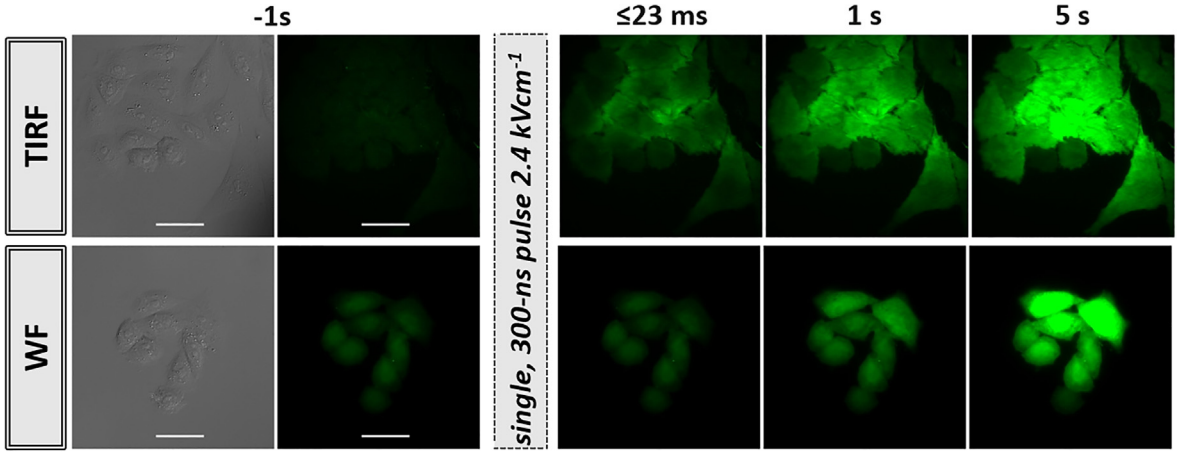

Fig. 11. The increased uptake of Ca^{2+} ions as observed in TIRF (top row) and widefield (lower row) modes. Cells loaded with Calbryte Ca^{2+} indicator were exposed in Tyrode's solution to a single 300 ns, 2.4 kVcm^{-1} pulse. Note the subplasmalemmal Ca^{2+} increased (TIRF mode) already at < 23 ms after the treatment. Scale bar is 20 μm.

camera, the actual time interval after pulse was even smaller for the upper part of the image. Such fast increase of subplasmalemmal Ca^{2+} provides evidence for electroporation of the lower membrane. This conclusion was further supported by the fact that the overall increase in cytosolic Ca^{2+} (Fig. 11, bottom row) became detectable later, consistently with prior observations that the Ca^{2+} diffusion through cytosol takes tens of milliseconds [81].

4. Discussion

In the present study we did not observe oxidation at the cathode-facing portion of cell membrane right after pulse delivery. It cannot be excluded that C11-BODIPY is not sensitive enough to detect slight lipid peroxidation. During optimization of staining and oxidation protocols we did not see oxidation evoked by CH-OOH removed prior to staining (so the dye was not in direct contact with CH-OOH but reacted to endogenously generated ROS). This matches the results obtained by Sakharov et al. [71] in which C11-BODIPY oxidation was barely visible in cells treated with 5 mM H_2O_2, washed and then stained. In another study the percentage of the oxidized algae cells exposed for 30 min to a mixture of BODIPY and 5 mM H_2O_2 was comparable to those obtained in a treatment in which the cells were exposed to H_2O_2, washed and then stained [41]. The lack of BP oxidation in our experiment can be explained by the application of different oxidizer with much smaller, non-lethal doses (data not shown) that were not sufficient for a prominent endogenous ROS generation or were immediately countered by antioxidant systems within CHO-K1 cells. On the other hand, degree of BP oxidation was detected when staining was performed in a presence of 25 μM CH-OOH which did not affect cell viability (data not shown). Moreover, FBS deprivation also increased green fluorescence of BODIPY, indicating that BP probe is indeed sensitive even to slight oxidation.

Anodic electric pulses enabled observation of C11-BODIPY oxidation. It may be argued if the presence of peroxidized lipids was required for BODIPY oxidation. Drummen et al. [15] observed a higher rate of BODIPY oxidation when increased amounts of polyunsaturated fatty acids (PUFAs) were present in mixed small, unilamellar vesicles (SUVs). The authors hypothesized that C11-$BODIPY^{581/591}$ is oxidized by chain-propagating species such as peroxyl and alkoxyl species, and not only directly from the oxidation-initiating species. However, further mass spectrometric analysis revealed that C11-BODIPY incubation in ethanol solution with 20 mM H_2O_2/250 μM $CuSO_4$ for 48 h resulted in complete probe oxidation giving emission spectra identical to oxidation with 20 mM AAPH or 20 mM MeO-AMVN [19]. On the other hand, Cheloni and Slaveykova (2013) noted similar oxidation in cells exposed for 30 min to a mixture of 2.5 μM C11-BODIPY/5 mM H_2O_2 and in cells exposed to the same concentration of H_2O_2, washed and then stained [18]. These results, together with the lack of oxidation in temperature-inactivated cells, led to the conclusion that C11-$BODIPY^{581/591}$ probe exhibits high stability in presence of peroxide and responds specifically to lipid oxidation [18]. Our results show that C11-BODIPY is stable in a solution of 100 μM cumene hydroperoxide for at least 90 min. With such defined conditions, C11-$BODIPY^{581/591}$ was demonstrated to be an excellent reporter for lipid oxidation as the fluorescence shift was visible only when there was lipid oxidation evoked in cells. However, the direct influence of high electric field on C11-BODIPY oxidation cannot be excluded.

It has been reported previously that the degree of BP oxidation can be affected by high-intensity light [21]. We found that the exposure of cells to laser excitation during sample focusing significantly affected the degree of BP oxidation observed (Fig. S2A). We did not observe oxidation when brightfield illumination was used for cells visualization. Therefore, to avoid focus-related bias we used brightfield illumination with DIC for the focus prior to acquisition.

Another limitation for C11-BODIPY oxidation analysis is photobleaching under high-intensity illumination [15]. We observed considerable photobleaching for long laser exposures. For millisecond-duration exposures, the photobleaching was minor in both oxidized and non-oxidized samples but not identical, therefore impacting the ratio (Fig. S2B). Our study was based on short measurements (maximum 9 images per cell), thus the dye instability was negligible. However, it should be considered and corrected for when continuous measurements are conducted.

Conclusions in the present study were made based on the C11-BODIPY oxidation measured right after pulse delivery. Occasionally, we also extended time between electropermeabilization and BP imaging and observed oxidation minutes after anodic electric pulses application (data not shown). Measurements made long after pulse delivery may carry information on secondary effects of electropermeabilization. Downstream effects of electropermeabilization can be diverse and affect cells on many levels starting from membrane resealing and ending with perturbations in cytoskeletal proteins [82]. They may also include PEFs-evoked intracellular ROS release from mitochondria [20]. However, these complex effects evoked by electropermeabilization are not the subject of present study and require a separate investigation. The hypothesis that oxidation-evoked leaky state of the membrane is required for electropermeabilization (see Introduction) is based on the assumption that oxidation precedes electropermeabilization. Hence, oxidation should be visible even at the time of pulse delivery and presumably at lower than electropermeabilization thresholds.

Early studies on milli- and microsecond PEFs revealed that electropermeabilization can induce the release of reactive oxygen species in CHO cells [21] and that ROS generation is not homogeneous on the cell surface but specific to the electropermeabilized region [23]. An increase in oxidation occurred only when electric field intensities were higher than electroporation threshold (enabling entry of the Direct-blue dye inside the cell) [23]. That was consistent with our data obtained for nanosecond pulses delivered to cells in the presence of Tyrode's solution (Fig. 7) or for both nano- and microsecond pulses when Tyrode's was replaced with a medium of lower conductivity (Fig. 10). Similarly, rapid peroxidation-related luminescence was observed in leukemia cells after application of millisecond pulse at 250 V/cm [83], which was demonstrated to be at a higher value than required for electropermeabilization [84]. The relationship between membrane permeability and oxidation was examined in recent theoretical studies [14]. It was demonstrated that permeability and conductance increase by several orders of magnitude in peroxidized bilayers. However, the conductance calculated in the study was too low to account for the entire range of values obtained experimentally [14]. Similar to our data, this result indicates that mechanisms other than lipid oxidation should be examined to fully explain the phenomenon of persistent electropermeabilization.

5. Conclusions

The relation between oxidation and electropermeabilization has been a subject of high interest for decades. One particularly intriguing question is whether oxidation-related leakiness of the membrane is necessary for persistent permeabilization. In the present study, we validated a novel method for the detection of lipid oxidation in the plasma membrane of living cells by combining C11-BODIPY staining with TIRF microscopy. We used this method to assess lipid peroxidation in CHO-K1 cells subjected to the action

of pulsed electric fields. Anodically applied electric pulses, delivered on a conductive ITO surface from a single electrode elevated above a cell, were sufficient to produce oxidation, but at electric field intensities above cell electropermeabilization thresholds to YO-PRO-1. Cathodically applied field produce no observable oxidation, but still produced permeabilization. The observed oxidation was nearly completely reduced when the cells were placed in a low conductive media suggesting that current was playing a key role in inducing membrane oxidation. However, the uptake of YO-PRO-1 was dramatically increased further decoupling lipid oxidation from electropermeabilization. This novel imaging method and its application towards investigation of rapid lipid peroxidation have shown that oxidation is unlikely a foundational mechanism for lasting permeabilization of cell membranes following pulse electric field exposure.

Acknowledgments

This work is a result of the research project financed by the National Science Center (Poland) No. 2017/27/N/NZ3/01110 (to Olga Michel) and AFOSR MURI grant FA9550-15-1-0517 (to Andrei Pakhomov). The publication costs were covered by the project financed from the funds granted by the MSHE (Poland) in the „Regional Initiative of Excellence" programme for the years 2019-2022, project no. 016/RID/2018/19, the amount of funding 11 998 121.30 PLN. We would like to acknowledge Polish-U.S. Fulbright Commission for granting Olga Michel the Fulbright Junior Research Award for an internship in the Frank Reidy Research Center for Bioelectrics. We would like to thank prof. Thomas Vernier for suggestions on C11-BODIPY staining protocols, fruitful discussions on PEFs-evoked lipid oxidation and stylistic corrections. The authors thank Dr. Bennett Ibey (AFRL) for comments and editing of the manuscript. We also thank Charles Rudkin for the linguistic corrections. The graphical abstract was prepared with the support of Servier Medical Art (https:// smart.servier.com) and GrabCad (https://grabcad.com, original objective figure prepared by Mark Richards).

Appendix A. Supplementary material

Supplementary data to this article can be found online at https://doi.org/10.1016/j.bioelechem.2019.107433.

References

[1] U. Reinhold, Electrochemotherapy for primary skin cancer and skin metastasis related to other malignancies, Anticancer. Drugs. 22 (2011) 711–718, https://doi.org/10.1097/CAD.0b013e32834618da.
[2] A. Szewczyk, J. Gehl, M. Daczewska, J. Saczko, S.K. Frandsen, J. Kulbacka, Calcium electroporation for treatment of sarcoma in preclinical studies, Oncotarget. 9 (2018), https://doi.org/10.18632/oncotarget.24352.
[3] R. Cadossi, M. Ronchetti, M. Cadossi, Locally enhanced chemotherapy by electroporation: clinical experiences and perspective of use of electrochemotherapy, Future Oncol. 10 (2014) 877–890, https://doi.org/10.2217/fon.13.235.
[4] J. Kulbacka, M.M. Daczewska, M. Dubińska-Magiera, A. Choromańska, N. Rembiałkowska, P.P. Surowiak, M. Kulbacki, M.M. Kotulska, J. Saczko, Doxorubicin delivery enhanced by electroporation to gastrointestinal adenocarcinoma cells with P-gp overexpression, Bioelectrochemistry. 100 (2014) 96–104, https://doi.org/10.1016/j.bioelechem.2014.03.013.
[5] M.L. Yarmush, A. Golberg, G. Serša, T. Kotnik, D. Miklavčič, Electroporation-based technologies for medicine: principles, applications, and challenges, Annu. Rev. Biomed. Eng. 16 (2014) 295–320, https://doi.org/10.1146/annurev-bioeng-071813-104622.
[6] A.C. Durieux, R. Bonnefoy, T. Busso, D. Freyssenet, In vivo gene electrotransfer into skeletal muscle: Effects of plasmid DNA on the occurrence and extent of muscle damage, J. Gene Med. 6 (2004) 809–816, https://doi.org/10.1002/jgm.534.
[7] J. Gehl, Gene electrotransfer in clinical trials, Methods Mol. Biol. 1121 (2014) 241–246, https://doi.org/10.1007/978-1-4614-9632-8_21.
[8] C. Rosazza, S. Haberl Meglic, A. Zumbusch, M.-P. Rols, D. Miklavcic, Gene electrotransfer: A mechanistic perspective, Curr. Gene Ther. 16 (2016) 98–129, https://doi.org/10.2174/1566523216666160331130040.
[9] J. Teissie, M.-P. Rols, Manipulation of cell cytoskeleton affects the lifetime of cell membrane electropermeabilization, Ann. N. Y. Acad. Sci. 720 (1994) 98–110, https://doi.org/10.1111/j.1749-6632.1994.tb30438.x.
[10] A.G. Pakhomov, A.M. Bowman, B.L. Ibey, F.M. Andre, O.N. Pakhomova, K.H. Schoenbach, Lipid nanopores can form a stable, ion channel-like conduction pathway in cell membrane, Biochem. Biophys. Res. Commun. 385 (2009) 181–186, https://doi.org/10.1016/j.bbrc.2009.05.035.
[11] M.P. Rols, J. Teissié, Electropermeabilization of mammalian cells. Quantitative analysis of the phenomenon, Biophys. J. 58 (1990) 1089–1098, https://doi.org/10.1016/S0006-3495(90)82451-6.
[12] Z.A. Levine, P.T. Vernier, Life cycle of an electropore: Field-dependent and field-independent steps in pore creation and annihilation, J. Membr. Biol. 236 (2010) 27–36, https://doi.org/10.1007/s00232-010-9277-y.
[13] W.F.D. Bennett, N. Sapay, D.P. Tieleman, Atomistic simulations of pore formation and closure in lipid bilayers, Biophys. J. 106 (2014) 210–219, https://doi.org/10.1016/j.bpj.2013.11.4486.
[14] L. Rems, M. Viano, M.A. Kasimova, D. Miklavčič, M. Tarek, The contribution of lipid peroxidation to membrane permeability in electropermeabilization: A molecular dynamics study, Bioelectrochemistry. 125 (2019) 46–57, https://doi.org/10.1016/J.BIOELECHEM.2018.07.018.
[15] P. Bonnafous, M.C. Vernhes, J. Teissié, B. Gabriel, The generation of reactive-oxygen species associated with long-lasting pulse-induced electropermeabilisation of mammalian cells is based on a non-destructive alteration of the plasma membrane, Biochim. Biophys. Acta - Biomembr. 1461 (1999) 123–134, https://doi.org/10.1016/S0005-2736(99)00154-6.
[16] M. Breton, L.M. Mir, Investigation of the chemical mechanisms involved in the electropulsation of membranes at the molecular level, Bioelectrochemistry. 119 (2018) 76–83, https://doi.org/10.1016/j.bioelechem.2017.09.005.
[17] M. Maccarrone, M.R. Bladergroen, N. Rosato, A.F. Agrò, Role of lipid peroxidation in electroporation-induced cell permeability, Biochem. Biophys. Res. Commun. 209 (1995) 417–425, https://doi.org/10.1006/bbrc.1995.1519.
[18] M. Yusupov, J. Van der Paal, E.C. Neyts, A. Bogaerts, Synergistic effect of electric field and lipid oxidation on the permeability of cell membranes, Biochim. Biophys. Acta - Gen. Subj. 2017 (1861) 839–847, https://doi.org/10.1016/J.BBAGEN.2017.01.030.
[19] P.T. Vernier, Z.A. Levine, Y.-H. Wu, V. Joubert, M.J. Ziegler, L.M. Mir, D.P. Tieleman, Electroporating fields target oxidatively damaged areas in the cell membrane, PLoS One. 4 (2009), https://doi.org/10.1371/journal.pone.0007966.
[20] O.N. Pakhomova, V.A. Khorokhorina, A.M. Bowman, R. Rodaite-Riševičiene, G. Saulis, S. Xiao, A.G. Pakhomov, Oxidative effects of nanosecond pulsed electric field exposure in cells and cell-free media, Arch. Biochem. Biophys. 527 (2012) 55–64, https://doi.org/10.1016/j.abb.2012.08.004.
[21] B. Gabriel, J. Teissié, Generation of reactive-oxygen species induced by electropermeabilization of Chinese hamster ovary cells and their consequence on cell viability, Eur. J. Biochem. 223 (1994) 25–33, https://doi.org/10.1111/j.1432-1033.1994.tb18962.x.
[22] L.C. Benov, P.A. Antonov, S.R. Ribarov, Oxidative damage of the membrane lipids after electroporation, Gen. Physiol. Biophys. 13 (1994) 85–97.
[23] B. Gabriel, J. Teissié, Spatial Compartmentation and time resolution of photooxidation of a cell membrane probe in electropermeabilized chinese hamster ovary cells, Eur. J. Biochem. 228 (1995) 710–718, https://doi.org/10.1111/j.1432-1033.1995.tb20314.x.
[24] B. Halliwell, J.M.C. Gutteridge, Gutteridge free radicals in biology and medicine, Oxford Univ. Press, 2007, p. 888 pp..
[25] J.M. Burns, W.J. Cooper, J.L. Ferry, D.W. King, B.P. DiMento, K. McNeill, C.J. Miller, W.L. Miller, B.M. Peake, S.A. Rusak, A.L. Rose, T.D. Waite, Methods for reactive oxygen species (ROS) detection in aqueous environments, Aquat. Sci. 74 (2012) 683–734, https://doi.org/10.1007/s00027-012-0251-x.
[26] R. Kohen, A. Nyska, Oxidation of biological systems: Oxidative stress phenomena, antioxidants, redox reactions, and methods for their quantification, Toxicol. Pathol. 30 (2002) 620–650, https://doi.org/10.1080/01926230290166724.
[27] M. Rajendran, Quinones as photosensitizer for photodynamic therapy: ROS generation, mechanism and detection methods, Photodiagnosis Photodyn. Ther. (2016), https://doi.org/10.1016/j.pdpdt.2015.07.177.
[28] T.P.A. Devasagayam, K.K. Boloor, T. Ramasarma, Methods for estimating lipid peroxidation: An analysis of merits and demerits, Indian J. Biochem. Biophys. 40 (2003) 300–308.
[29] E. Shacter, Quantification and significance of protein oxidation in biological samples, Drug Metab. Rev. (2000) 307–326, https://doi.org/10.1081/DMR-100102336.
[30] M.J.C. Long, J.R. Poganik, S. Ghosh, Y. Aye, Subcellular redox targeting: bridging in vitro and in vivo chemical biology, ACS Chem. Biol. 12 (2017) 586–600, https://doi.org/10.1021/acschembio.6b01148.
[31] B. Barriuso, I. Astiasarán, D. Ansorena, A review of analytical methods measuring lipid oxidation status in foods: a challenging task, Eur. Food Res. Technol. 236 (2013) 1–15, https://doi.org/10.1007/s00217-012-1866-9.
[32] A. Kaur, J.L. Kolanowski, E.J. New, Reversible Fluorescent Probes for Biological Redox States, Angew. Chemie - Int. Ed. 55 (2016) 1602–1613, https://doi.org/10.1002/anie.201506353.
[33] T. Yan, X. Jiang, H.J. Zhang, S. Li, L.W. Oberley, Use of commercial antibodies for detection of the primary antioxidant enzymes, Free Radic. Biol. Med. 25 (1998) 688–693, https://doi.org/10.1016/S0891-5849(98)00112-9.

[34] M.N. Alam, N.J. Bristi, M. Rafiquzzaman, Review on in vivo and in vitro methods evaluation of antioxidant activity, Saudi Pharm. J. 21 (2013) 143–152, https://doi.org/10.1016/j.jsps.2012.05.002.
[35] O. Blokhina, E. Virolainen, K.V. Fagerstedt, Antioxidants, oxidative damage and oxygen deprivation stress: a review, Ann. Bot. 91 (2003) 179–194, Spec No.
[36] A.M. Pisoschi, C. Cimpeanu, G. Predoi, Electrochemical methods for total antioxidant capacity and its main contributors determination: a review, Open Chem. 13 (2015), https://doi.org/10.1515/chem-2015-0099.
[37] A.M. Pisoschi, G.P. Negulescu, Methods for total antioxidant activity determination: a review, Biochem. Anal. Biochem. 01 (2012), https://doi.org/10.4172/2161-1009.1000106.
[38] G.P. Drummen, L.C. van Liebergen, J.A. Op den Kamp, J.A. Post, C11-BODIPY581/591, an oxidation-sensitive fluorescent lipid peroxidation probe: (micro)spectroscopic characterization and validation of methodology, Free Radic. Biol. Med. 33 (2002) 473–490, https://doi.org/10.1016/S0891-5849(02)00848-1.
[39] M. Baruah, W. Qin, N. Basarić, W.M. De Borggraeve, N. Boens, BODIPY-based hydroxyaryl derivatives as fluorescent pH probes, J. Org. Chem. 70 (2005) 4152–4157, https://doi.org/10.1021/jo0503714.
[40] N. Boens, V. Leen, W. Dehaen, Fluorescent indicators based on BODIPY, Chem. Soc. Rev. 41 (2012) 1130–1172, https://doi.org/10.1039/C1CS15132K.
[41] G. Cheloni, V.I. Slaveykova, Optimization of the C11-BODIPY 581/591 dye for the determination of lipid oxidation in Chlamydomonas reinhardtii by flow cytometry, Cytom. Part A. 83 (2013), https://doi.org/10.1002/cyto.a.22338, n/a-n/a.
[42] G.P.C. Drummen, B.M. Gadella, J.A. Post, J.F. Brouwers, Mass spectrometric characterization of the oxidation of the fluorescent lipid peroxidation reporter molecule C11-BODIPY581/591, Free Radic. Biol. Med. (2004), https://doi.org/10.1016/j.freeradbiomed.2004.03.014.
[43] Y. Yoshida, S. Shimakawa, N. Itoh, E. Niki, Action of DCFH and BODIPY as a probe for radical oxidation in hydrophilic and lipophilic domain, Free Radic. Res. 37 (2003) 861–872, https://doi.org/10.1080/1071576031000148736.
[44] E.H.W. Pap, G.P.C. Drummen, V.J. Winter, T.W.A. Kooij, P. Rijken, K.W.A. Wirtz, J.A.F. Op Den Kamp, W.J. Hage, J.A. Post, Ratio-fluorescence microscopy of lipid oxidation in living cells using C11-BODIPY(581/591), FEBS Lett. (1999), https://doi.org/10.1016/S0014-5793(99)00696-1.
[45] M.L. MacDonald, I.V.J. Murray, P.H. Axelsen, Mass spectrometric analysis demonstrates that BODIPY 581/591 C11 overestimates and inhibits oxidative lipid damage, Free Radic. Biol. Med. (2007), https://doi.org/10.1016/j.freeradbiomed.2007.01.038.
[46] E.H.W. Pap, G.P.C. Drummen, J.A. Post, P.J. Rijken, K.W.A. Wirtz, [54] Fluorescent fatty acid to monitor reactive oxygen in single cells, Methods Enzymol. 319 (2000) 603–612, https://doi.org/10.1016/S0076-6879(00)19056-1.
[47] A.L. Mattheyses, S.M. Simon, J.Z. Rappoport, Imaging with total internal reflection fluorescence microscopy for the cell biologist, J. Cell Sci. 123 (2010) 3621–3628, https://doi.org/10.1242/jcs.056218.
[48] D. Axelrod, Biophysical Tools for Biologists - chap 8: Total Internal Reflection Microscopy, Elsevier (2008), https://doi.org/10.1016/S0091-679X(08)00607-9.
[49] D. Axelrod, Total internal reflection fluorescence microscopy, Encycl. Cell Biol. (2015), https://doi.org/10.1016/B978-0-12-394447-4.20089-8.
[50] M.A. Partridge, E.E. Marcantonio, Initiation of attachment and generation of mature focal adhesions by integrin-containing filopodia in cell spreading, Mol. Biol. Cell. (2006), https://doi.org/10.1091/mbc.E06-06-0496.
[51] G. Danuser, C.M. Waterman-Storer, Quantitative fluorescent speckle microscopy of cytoskeleton dynamics, Annu. Rev. Biophys. Biomol. Struct. (2006), https://doi.org/10.1146/annurev.biophys.35.040405.102114.
[52] M.C. Adams, A. Matov, D. Yarar, S.L. Gupton, G. Danuser, C.M. Waterman-Storer, Signal analysis of total internal reflection fluorescent speckle microscopy (TIR-FSM) and wide-field epi-fluorescence FSM of the actin cytoskeleton and focal adhesions in living cells, J. Microsc. (2004), https://doi.org/10.1111/j.0022-2720.2004.01408.x.
[53] J. Schmoranzer, S.M. Simon, Role of microtubules in fusion of post-Golgi vesicles to the plasma membrane, Mol. Biol. Cell. (2003), https://doi.org/10.1091/mbc.E02-08-0500.
[54] A. Demuro, I. Parker, Imaging the activity and localization of single voltage-gated Ca 2+ channels by total internal reflection fluorescence microscopy, Biophys. J. (2004), https://doi.org/10.1016/S0006-3495(04)74373-8.
[55] A.N. Weiss, A. Anantharam, M.A. Bittner, D. Axelrod, R.W. Holz, Lumenal protein within secretory granules affects fusion pore expansion, Biophys. J. (2014), https://doi.org/10.1016/j.bpj.2014.04.064.
[56] J. Schmoranzer, M. Goulian, D. Axelrod, S.M. Simon, Imaging constitutive exocytosis with total internal reflection fluorescence microscopy, J. Cell Biol. (2000), https://doi.org/10.1083/jcb.149.1.23.
[57] I. Akopova, S. Tatur, M. Grygorczyk, R. Luchowski, I. Gryczynski, Z. Gryczynski, J. Borejdo, R. Grygorczyk, Imaging exocytosis of ATP-containing vesicles with TIRF microscopy in lung epithelial A549 cells, Purinergic Signal. 8 (2012) 59–70, https://doi.org/10.1007/s11302-011-9259-2.
[58] J. Yang, Y.L. Xiong, Inhibition of lipid oxidation in oil-in-water emulsions by interface-adsorbed myofibrillar protein, J. Agric. Food Chem. (2015), https://doi.org/10.1021/acs.jafc.5b03377.
[59] L.J. Johnston, Nanoscale imaging of domains in supported lipid membranes, Langmuir. (2007), https://doi.org/10.1021/la070108t.
[60] O.N. Pakhomova, B. Gregory, I. Semenov, A.G. Pakhomov, Calcium-mediated pore expansion and cell death following nanoelectroporation, Biochim. Biophys. Acta - Biomembr. 2014 (1838) 2547–2554, https://doi.org/10.1016/J.BBAMEM.2014.06.015.
[61] E.C. Gianulis, C. Labib, G. Saulis, V. Novickij, O.N. Pakhomova, A.G. Pakhomov, Selective susceptibility to nanosecond pulsed electric field (nsPEF) across different human cell types, Cell. Mol. Life Sci. 74 (2017) 1741–1754, https://doi.org/10.1007/s00018-016-2434-4.
[62] C.A. Tyson, J.M. Frazier, In vitro toxicity indicators, first ed., Academic Press, 2013, ISBN: 9780080924403 (accessed June 14, 2019).
[63] N. Gamper, J.D. Stockand, M.S. Shapiro, The use of Chinese hamster ovary (CHO) cells in the study of ion channels, J. Pharmacol. Toxicol. Meth. 51 (2005) 177–185, https://doi.org/10.1016/j.vascn.2004.08.008.
[64] I. Semenov, S. Xiao, O.N. Pakhomova, A.G. Pakhomov, Recruitment of the intracellular Ca2+ by ultrashort electric stimuli: The impact of pulse duration, Cell Calcium. 54 (2013) 145–150, https://doi.org/10.1016/j.ceca.2013.05.008.
[65] I. Semenov, S. Xiao, A.G. Pakhomov, Primary pathways of intracellular Ca2 + mobilization by nanosecond pulsed electric field, Biochim. Biophys. Acta - Biomembr. 2013 (1828) 981–989, https://doi.org/10.1016/j.bbamem.2012.11.032.
[66] A.G. Pakhomov, E. Gianulis, P.T. Vernier, I. Semenov, S. Xiao, O.N. Pakhomova, Multiple nanosecond electric pulses increase the number but not the size of long-lived nanopores in the cell membrane, Biochim. Biophys. Acta - Biomembr. 2015 (1848) 958–966, https://doi.org/10.1016/j.bbamem.2014.12.026.
[67] E.C. Gianulis, A.G. Pakhomov, Gadolinium modifies the cell membrane to inhibit permeabilization by nanosecond electric pulses, Arch. Biochem. Biophys. 570 (2015) 1–7, https://doi.org/10.1016/j.abb.2015.02.013.
[68] Indium Tin Oxide, (n.d.). (accessed June 26, 2019). http://www.mit.edu/~6.777/matprops/ito.htm.
[69] H.A. Ryan, S. Hirakawa, E. Yang, C. Zhou, S. Xiao, High-voltage, multiphasic, nanosecond pulses to modulate cellular responses, IEEE Trans. Biomed. Circuits Syst. 12 (2018) 338–350, https://doi.org/10.1109/TBCAS.2017.2786586.
[70] J. Schindelin, I. Arganda-Carreras, E. Frise, V. Kaynig, M. Longair, T. Pietzsch, S. Preibisch, C. Rueden, S. Saalfeld, B. Schmid, J.-Y. Tinevez, D.J. White, V. Hartenstein, K. Eliceiri, P. Tomancak, A. Cardona, Fiji: an open-source platform for biological-image analysis, Nat. Meth. 9 (2012) 676–682, https://doi.org/10.1038/nmeth.2019.
[71] D.V. Sakharov, E.D.R. Elstak, B. Chernyak, K.W.A. Wirtz, Prolonged lipid oxidation after photodynamic treatment. Study with oxidation-sensitive probe C11-BODIPY581/591, FEBS Lett. 579 (2005) 1255–1260, https://doi.org/10.1016/j.febslet.2005.01.024.
[72] J.F. Koster, R.G. Slee, C.E. Essed, H. Stam, Studies on cumene hydroperoxide-induced lipid peroxidation in the isolated perfused rat heart, J. Mol. Cell. Cardiol. 17 (1985) 701–708, https://doi.org/10.1016/S0022-2828(85)80069-9.
[73] A. Linden, M. Gülden, H.J. Martin, E. Maser, H. Seibert, Peroxide-induced cell death and lipid peroxidation in C6 glioma cells, Toxicol. Vitr. 22 (2008) 1371–1376, https://doi.org/10.1016/j.tiv.2008.02.003.
[74] A.G. Pakhomov, R. Shevin, J.A. White, J.F. Kolb, O.N. Pakhomova, R.P. Joshi, K.H. Schoenbach, Membrane permeabilization and cell damage by ultrashort electric field shocks, Arch. Biochem. Biophys. 465 (2007) 109–118, https://doi.org/10.1016/j.abb.2007.05.003.
[75] J. Newman, K.E. Thomas-Alyea, Electrochemical systems, Inc Publication, A John Wiley & Sons, 2004.
[76] P.E. Crago, P.H. Peckham, J.T. Mortimer, J.P. Van Der Meulen, The choice of pulse duration for chronic electrical stimulation via surface, nerve, and intramuscular electrodes, Ann. Biomed. Eng. 2 (1974) 252–264, https://doi.org/10.1007/BF02368496.
[77] A. Silve, I. Leray, C. Poignard, L.M. Mir, Impact of external medium conductivity on cell membrane electropermeabilization by microsecond and nanosecond electric pulses, Sci. Rep. 6 (2016), https://doi.org/10.1038/srep19957.
[78] K.J. Müller, V.L. Sukhorukov, U. Zimmermann, Reversible electropermeabilization of mammalian cells by high-intensity, ultra-short pulses of submicrosecond duration, J. Membr. Biol. 184 (2001) 161–170, https://doi.org/10.1007/s00232-001-0084-3.
[79] E.C. Gianulis, M. Casciola, S. Xiao, O.N. Pakhomova, A.G. Pakhomov, Electropermeabilization by uni- or bipolar nanosecond electric pulses: The impact of extracellular conductivity, Bioelectrochemistry 119 (2018) 10–19, https://doi.org/10.1016/j.bioelechem.2017.08.005.
[80] A. Silve, I. Leray, M. Leguèbe, C. Poignard, L.M. Mir, Cell membrane permeabilization by 12-ns electric pulses: Not a purely dielectric, but a charge-dependent phenomenon, Bioelectrochemistry. 106 (2015) 369–378, https://doi.org/10.1016/j.bioelechem.2015.06.002.
[81] I. Semenov, C. Zemlin, O.N. Pakhomova, S. Xiao, A.G. Pakhomov, Diffuse, non-polar electropermeabilization and reduced propidium uptake distinguish the effect of nanosecond electric pulses, Biochim. Biophys. Acta - Biomembr. 2015 (1848) 2118–2125, https://doi.org/10.1016/j.bbamem.2015.06.018.
[82] T. Kotnik, L. Rems, M. Tarek, D. Miklavčič, Membrane Electroporation and Electropermeabilization: Mechanisms and Models, Annu. Rev. Biophys. 48 (2019) 63–91, https://doi.org/10.1146/annurev-biophys-052118-115451.
[83] M. Maccarrone, C. Fantini, A.F. Agrò, N. Rosato, Kinetics of ultraweak light emission from human erythroleukemia K562 cells upon electroporation, Biochim. Biophys. Acta - Biomembr. 1414 (1998) 43–50, https://doi.org/10.1016/S0005-2736(98)00150-3.
[84] A. Maček-Lebar, D. Miklavčič, Cell electropermeabilization to small molecules in vitro: control by pulse parameters, Radiol. Oncol. 35 (2001) 193–202.